Available online at www.sciencedirect.com

ScienceDirect

Ceramics International 40 (2014) 1699–1707

CERAMICS INTERNATIONAL

www.elsevier.com/locate/ceramint

# In situ elastic modulus evaluation of $Al_2O_3$–MgO refractory castables

T.M. Souza[a,*], A.P. Luz[a], M.A.M. Brito[b], V.C. Pandolfelli[a]

[a]Federal University of São Carlos, Materials Engineering Department, Materials Microstructure Engineering Group (GEMM), FIRE Associate Laboratory Rod. Washington Luiz, km 235, São Carlos, SP 13565-905, Brazil

[b]Magnesita Refratários S.A., Research and Development Center, Praça Louis Ensch, 240 Contagem, MG, Brazil

Received 2 July 2013; received in revised form 11 July 2013; accepted 12 July 2013
Available online 20 July 2013

**Abstract**

Elastic modulus evaluation is a simple and very accurate technique to investigate refractory castable behavior during curing, drying and firing steps. Therefore, analyzing this property might be useful to assess microstructural changes in $Al_2O_3$–MgO systems, where *in situ* transformations play an important role at high temperature. Considering this aspect, dead-burnt magnesia containing refractory castables with 0 wt%, 2 wt%, 4 wt % or 6 wt% of calcium aluminate cement and 1 wt% of fumed silica, as well as an additional cement-free composition containing a caustic magnesia source (with higher reactivity) were evaluated using hot elastic modulus measurements, thermodynamic calculations and XRD analysis. The cement-free castables attested that the greater the brucite content, the higher the drop in the elastic modulus. On the other hand, $MgAl_2O_4$ formation increased the sample′s stiffness, but the presence of caustic magnesia did not significantly affect the elastic behavior at high temperatures. For the cement bonded systems, reactions between CaO, $SiO_2$ and $Al_2O_3$ resulted in a remarkable increase in the elastic modulus above 800 °C, whereas at higher temperatures liquid phase generation spoiled the castable′s properties. Thermodynamic calculations indicated that reducing the cement content, a lower amount of glassy phase was generated in the matrix, leading to a higher *E* value after the cooling stage. The elastic modulus profile for the second thermal cycle also suggested that a glassy phase transition occurred above 1000 °C for the evaluated castables.



*Keywords:* D. MgO; D. Spinel; Elastic modulus; Refractory castables

## 1. Introduction

There has been increasing interest in using dynamic and non-destructive methods such as the resonant bar and ultrasonic echography techniques to evaluate the elastic modulus of refractory materials [1–3]. Compared with static tests, the dynamic ones have the additional advantage of maintaining the material′s integrity after measuring [2]. As a result, the same sample can be used to evaluate the Young′s modulus with the temperature providing insights of the *in situ* chemical and structural evolutions. Furthermore, the simplicity and accuracy of this sort of method has made it suitable to investigate refractory castables, whose mechanical strength is affected by microstructural changes during the curing, drying and firing steps.

From a theoretical point of view, the elastic modulus can be obtained by the second-order derivative of the inter-atomic potential, indicating that it is closely related to the atomic bond strength [3]. Consequently, in multiphase materials with complex heterogeneous microstructures, the elastic constants are also strongly dependent on the crystalline structure and flaws, such as porosity and cracks.

For $Al_2O_3$–MgO cement free compositions, two *in situ* phase transformations must be highlighted: brucite [$Mg(OH)_2$] formation and decomposition, and spinel generation. The first one usually takes place when MgO is in contact with water during the mixing, curing and drying processing steps, leading to a remarkable 2.5-fold volumetric expansion [4,5]. The second occurs above 1000 °C by the reaction between alumina

*Corresponding author at: Tel.: +55 16 33518253; fax: +55 16 33615404.
*E-mail address:* uaitiago@gmail.com (T.M. Souza).

0272-8842/$ - see front matter © 2013 Elsevier Ltd and Techna Group S.r.l. All rights reserved.
http://dx.doi.org/10.1016/j.ceramint.2013.07.066

and fine magnesia contained in the matrix, which can also give rise to high volumetric expansion [6]. These expansive reactions or even the thermal expansion mismatch among the castable phases can lead either to interfacial separation between aggregates and matrix or to microcracks, affecting the material′s performance. Therefore, both reactions can play a role by increasing or decreasing the castable′s stiffness, depending on the overall expansion and microstructural features (such as the available porosity).

Concerning the MgO hydration, a recent study using elastic modulus measurements pointed out that the selection of optimized amounts of calcium aluminate cement or fumed silica can be an efficient route to inhibit the hydration drawbacks for different magnesia sources [7]. The authors also suggested that when compared with mechanical tests, the resonant bar technique can detect crack formation at an earlier stage and, thus it is a suitable procedure to evaluate the magnesia′s hydration damage.

Over the latest years, volumetric expansion associated with $MgAl_2O_4$ formation has also been extensively studied [6,8–11]. However, less attention has been paid to the effect of this transformation on the elastic properties of refractories. There is little research presented in the scientific literature focusing on the evaluation of the elastic modulus behavior of $Al_2O_3$–MgO castables [12,13]. Furthermore, this work did not consider the coupled effects derived from the presence of different magnesia sources and cement or fumed silica, as the interaction of these components affect the overall expansion of the refractories [6,10].

For $Al_2O_3$–MgO castables containing calcium aluminate cement (CAC), two additional *in situ* transformations are also present during the sample′s heating up step: $CaAl_4O_7$ ($CA_2$) and $CaAl_{12}O_{19}$ ($CA_6$) formation [6,14]. The $CA_2$ generation is an expansive reaction detected at temperatures higher than 1100 °C. However, when fumed silica is added to the refractory compositions, CaO can also react with $Al_2O_3$ and $SiO_2$ to form glassy phases, reducing the amount of $CA_2$ generated and, consequently, its expansive result [10]. If a great amount of alumina is available, $CA_2$ phase is completely consumed at higher temperatures leading to $CA_6$ formation, which also results in a remarkable volumetric expansion (3.01%) [12], affecting the castables mechanical properties.

Braulio et al. evaluated these previous transformations and suggested engineered expansion routes for the design of advanced alumina–magnesia castables [6,8–11]. The role of many parameters on the castables *in situ* expansion was evaluated, such as the cement and silica fume contents, the magnesia source and the use of mineralizer and densifier compounds. On the other hand, in addition to the interesting benefits associated with the expansion control, novel insights about the effect of those components could be attained if *in situ* elastic modulus measurements would be used to investigate alumina–magnesia castables.

In order to provide additional information about the effect of such *in situ* transformations on the castable′s stiffness and better understand these reactions, the evaluation of the elastic modulus as a function of the temperature would be very useful. Therefore, the aim of this study was to evaluate the influence of different calcium aluminate cement contents (0 wt%, 2 wt%, 4 wt% or 6 wt%), 1 wt% of fumed silica and two distinct magnesia sources (a dead-burnt or a caustic magnesia one) on the elastic modulus behavior of $Al_2O_3$–MgO castables. Thermodynamic calculations and XRD analysis were also carried out in order to better understand and explain the transformations observed in the attained elastic modulus curves ($E$ versus temperature).

## 2. Materials and techniques

As conducted by Braulio et al. [6], vibratable alumina–magnesia castable compositions containing different calcium aluminate cement (Secar 71, Kerneos, France) contents were designed according to Alfred′s particle packing model ($q=0.26$) [15]. Coarse tabular alumina was added as aggregates ($d\leq 6$ mm, Almatis, USA) and the matrix fraction comprised magnesia, reactive alumina (CL370, Almatis, USA), fine tabular alumina (≤200 μm, Almatis, USA) and 1 wt% silica fume (971U, Elkem, Norway). In order to assess the magnesia reactivity effect on spinel formation, dead-burnt (DB) and caustic magnesia (CM) (Magnesita Refratários S.A., Brazil) with specific surface areas of 1.1 $m^2/g$ and 11.1 $m^2/g$, respectively, were added to the cement free castable. The magnesia′s physical properties and chemical compositions are presented in Table 1.

The castable dispersion was carried out by adding 0.2 wt% of a polycarboxylate based dispersant (Basf, Germany) and the water content for suitable casting was defined based on an initial 80% vibra-flow value. General information regarding the compositions is presented in Table 2. After mixing and casting, all castable samples were cured for 24 h in a climatic chamber (Vöetsch 2020, Germany) at 50 °C in an environment with relative humidity close to 80% and dried at 110 °C for 24 h.

The hot elastic modulus was evaluated using dry prismatic samples (25 mm × 25 mm × 150 mm). These measurements were carried out according to ASTM C 1198-91 using the resonance bar technique (Scanelastic equipment, ATCP, Brazil), which is based on the sample excitation and by

Table 1
Physical properties and chemical compositions of the selected magnesia sources (DB: dead-burnt and CM: caustic magnesia).

| MgO source | | DB | CM |
|---|---|---|---|
| Physical and chemical properties | SSA ($m^2/g$) | 1.1 | 11.1 |
| | $D_{10}$ (μm) | 0.55 | 2.05 |
| | $D_{50}$ (μm) | 7.76 | 20.14 |
| | $D_{90}$ (μm) | 35.48 | 52.19 |
| | $\rho$ ($g/cm^3$) | 3.53 | 3.20 |
| Chemical composition (wt%) | MgO | 98.17 | 94.73 |
| | CaO | 0.84 | 0.42 |
| | $SiO_2$ | 0.33 | 1.58 |
| | $Al_2O_3$ | 0.12 | 0.35 |
| | $Fe_2O_3$ | 0.41 | 2.06 |
| | MnO | 0.13 | 0.86 |
| | $CaO/SiO_2$ | 2.54 | 0.27 |

SSA = specific surface area. $D_{90}$, $D_{50}$ and $D_{10}$ = equivalent spherical particle diameter below 90%, 50% and 10%, respectively; $\rho$ = density.

Table 2
Refractory castable compositions evaluated in this work.

| Raw materials | Content (wt%) | | | | |
|---|---|---|---|---|---|
| | 6C | 4C | 2C | 0C | CM-0C |
| Tabular alumina ($d \leq 6$ mm) | 80 | 80 | 80 | 80 | 80 |
| Reactive alumina (CL370) | 7 | 9 | 11 | 7 | 7 |
| Magnesia (DB or CM) | 6 | 6 | 6 | 6 | 6 |
| Fumed silica (971U) | 1 | 1 | 1 | 1 | 1 |
| Calcium aluminate cement (Secar 71) | 6 | 4 | 2 | 0 | 0 |
| Tabular alumina ($d < 45$ μm) | 0 | 0 | 0 | 6 | 6 |
| Water | 4.2 | 4.1 | 4.0 | 4.1 | 5.1 |

detecting the correspondent vibration spectrum, using piezoelectric transducers. In such experiments, wide frequency scanning is performed in order to excite and capture the natural resonance frequencies of the ceramic bars. Elastic modulus is calculated based on the resulted vibration spectrum applying Pickett equations, which correlates the elastic modulus, the natural vibration frequencies and the sample dimensions [16]. For the fundamental flexural frequency of a rectangular bar, the Young′s modulus is given by:

$$E = 0.9465 \frac{mf_f^2}{b} \times \frac{L^3}{t^3} \times T_1 \quad (1)$$

where, $E$ is the Young′s modulus (Pa), $m$ the mass (g), $b$ the width (mm), $L$ the length (mm), $t$ the thickness (mm), $f_f$ the fundamental resonance frequency of the bar in flexure (Hz), and $T_1$ the correction factor for fundamental flexural mode to account for the finite thickness of the bar, Poisson′s ratio and others. The tests were conducted in the 50–1400 °C temperature range in air ($pO_2 = 0.21$ atm) with heating and cooling rates of 2 °C/min. Various experiments using the selected compositions were carried out and the collected results shown very good reliability (standard deviation lower than 5%).

After two thermal cycles of elastic modulus measurements up to 1400 °C, the refractory castables were ground ($dp < 45$ μm) in a tungsten carbide mill (AMEF, model AMP1-M, Brazil) and analyzed using the X-ray diffraction technique (Bruker equipment, model D8 Focus, Germany) and EVA software. The 0C and 6C fine grain matrices were also prepared (considering only the fine particles lower than 100 μm) and their phase composition evaluated after drying at 110 °C and firing at 800 °C, 1000 °C, 1200 °C and 1500 °C. General information regarding the castable matrices is presented in Table 3.

Thermodynamic simulations were also carried out using FactSage™ software [version 6.3.1, Thermofact/CRCT (Montreal) and GTT-Technologies (Aachen), Federal University of São Carlos] aiming to predict the castable′s phase composition, the liquid-phase content and its composition and viscosity from 1000 °C up to 1500 °C under a total pressure of 1 atm. FactPa.s. and FToxid databases and Equilib and Viscosity modules were selected for this evaluation. The simulations were performed considering the castable′s overall composition (Table 2) and their fine grain matrices (Table 3).

Table 3
Refractory matrix compositions evaluated by XRD analysis and the thermodynamic simulations.

| Raw materials | Content (wt%) | | | |
|---|---|---|---|---|
| | 6C | 4C | 2C | 0C |
| Reactive alumina (CL370) | 35 | 35 | 35 | 35 |
| Fumed silica (971 U) | 5 | 5 | 5 | 5 |
| Magnesia | 30 | 30 | 30 | 30 |
| Calcium aluminate cement (Secar 71) | 30 | 20 | 10 | 0 |
| Tabular alumina ($d < 45$ μm) | 0 | 10 | 20 | 30 |

## 3. Results and discussion

### 3.1. Effect of different MgO sources

Concerning cement free castables, a greater amount of water is usually available to react with magnesia during the processing steps [7], therefore the amount of $Mg(OH)_2$ generated is higher and consequently provides a more accurate evaluation of brucite′s decomposition effect on the elastic modulus. Additionally, in this case, $MgAl_2O_4$ is the main phase that crystallizes at high temperatures, making it possible to investigate the magnesia reactivity effect on the materials' properties.

Fig. 1a presents the elastic modulus results for the designed cement free compositions. Based on the $E$ curves, the CM-0C castable (which contained the caustic MgO source) presented lower $E$ values at all evaluated temperatures. This behavior is related to the greater water content required for a suitable casting of this composition (as highlighted in Table 2), which reduces the castable′s mechanical strength and elastic modulus. From 50 °C to ~370 °C, the sample′s stiffness remained constant, but a substantial and continuous drop in the $E$ values was observed up to 1000 °C. According to the X-ray results presented in Table 4, at 110 °C the 0C fine matrix was mainly comprised of $Al_2O_3$, MgO and $Mg(OH)_2$. As the magnesium hydroxide decomposition usually initiates above 350 °C and has already been completed at 600 °C [5,17], the additional decrease observed in the elastic modulus above 600 °C might be associated with the crack formation due to the water vapor release and the temperature increase (Fig. 1a). This statement is strengthened when compared with the other $E \times T$ profiles presented in this paper.

Although some significant differences between the caustic and dead burnt magnesia containing compositions were noticed in the elastic modulus curves, the E percentual change confirmed that a higher amount of brucite was generated for the CM-0C castable and, consequently, the stiffness percentage drop was higher (Fig. 1b).

It can be clearly seen that the castable′s stiffness reached their lowest values at temperatures slightly higher than 1000 °C (Fig. 1a), indicating that the amount of forsterite ($Mg_2SiO_4$) generated in the fine matrix at 800 °C was not enough to increase the $E$ values (Table 4). On the other hand, above 1000 °C the elastic modulus increased up to 1400 °C as a consequence of the sintering process and spinel formation (Fig. 1a; Table 4). It was observed that crystallization of $MgAl_2O_4$ can lead to an increase

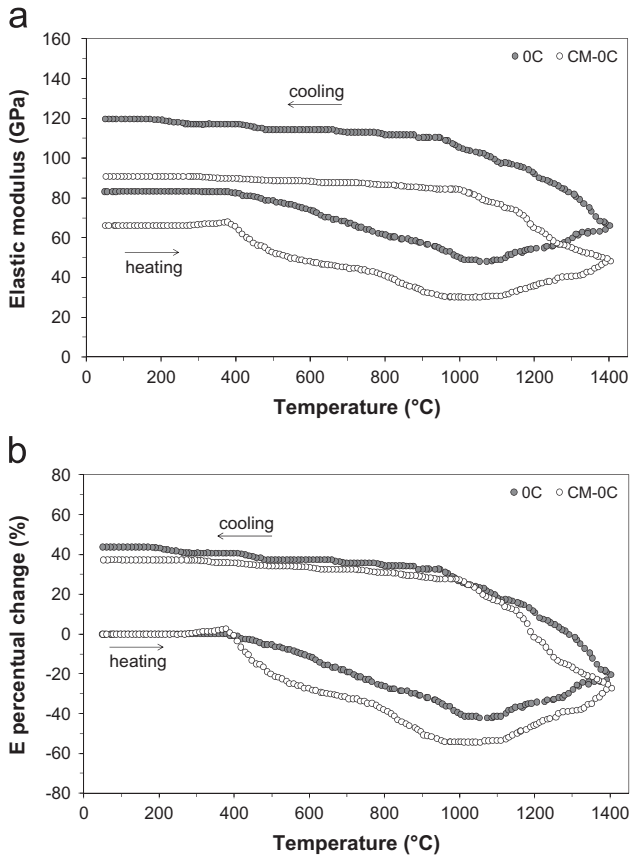


Fig. 1. (a) *In situ* elastic modulus and (b) elastic modulus percentual change as a function of the temperature for the cement free castables containing dead-burnt (0C) or caustic magnesia (CM-0C). Samples obtained after curing (50 °C/24 h) and drying (110 °C/24 h) steps.

Table 4
Phase changes in the matrix of the 0C castable obtained by X-ray diffraction analysis[a].

| Crystalline phases | Composition 0C | | | | |
|---|---|---|---|---|---|
| | 110 °C | 800 °C | 1000 °C | 1200 °C | 1500 °C |
| MgO | ****** | ***** | **** | *** | |
| $Al_2O_3$ | ****** | ***** | **** | *** | |
| $Mg(OH)_2$ | * | | | | |
| $Mg_2SiO_4$ | | * | * | * | * |
| $MgAl_2O_4$ | | | ** | *** | ****** |

[a]The number of asterisks indicates the phase proportion estimated by means of the main difraction peak intensity.

in the *E* values. However, it should be highlighted that some authors reported that *in situ* spinel based castables without cement and containing silica fume usually present a drop in the hot modulus of rupture above 1000 °C due to the high volumetric expansion and, consequently, the formation of microcracks and some liquid formation [18]. Hence, the presence of these flaws can counterbalance the rate of elastic modulus increase above 1000 °C (Fig. 1a).

Aiming to figure out the transformations previously indicated, especially the liquid formation, thermodynamic calculations were used to predict the phases under equilibrium condition at high temperature. Regarding the overall castable composition, the simulations indicated the presence of $Al_2O_3$ and $MgAl_2O_4$ as the main phases (Fig. 2a), which was consistent with those identified in the collected samples. The calculations did not show any liquid phases for the cement free castable, but the formation of sapphirine ($M_4A_5S_2$) and mullite ($A_3S_2$). Concerning the equilibrium phase diagram, a composition in the alumina–spinel–mullite compatibility triangle will produce the first liquid only above 1580 °C. Nevertheless, Sandberg et al. stated that compositions in this compatibility triangle soften at much lower temperatures and no mullite was detected at 1500 °C, suggesting that fumed silica should be present as a glassy phase [19].

In spite of the absence of liquid phases in the thermodynamic predictions for the castable′s overall composition (Fig. 2a), liquid formation was indicated to be found in the fine grain matrix above 1300 °C (Fig. 2b). The amount of liquid in the matrix reached 7.38 wt% at 1500 °C, comprising 19.5% $Al_2O_3$, 35.6% MgO, 44.9% $SiO_2$ in its composition and viscosity of 0.52 Pa. s. Spinel, forsterite and sapphirine was also contained in the matrix, but according to the experimental results (XRD data, Table 4), this later phase was not detected in the evaluated samples.

When the elastic modulus results of samples presented in Fig. 1 were analyzed considering the thermodynamic predictions (Fig. 2), it was clear that glassy phases might have been formed during the heat treatments. The differences between the experiments and the simulations can be better understood when two important aspects are considered: (i) changes in the local domain composition might occur throughout the microstructure, leading to the formation of liquid at lower temperatures; and (ii) the impurities of the raw materials were not considered in the calculations.

Comparing the castables containing dead-burnt (0C) and caustic magnesia (CM-0C), the attained E profiles did not show any considerable change at high temperatures (Fig. 1a). This feature indicates that the reactivity of fine magnesia sources did not significantly affect the phase transformations and the overall elastic modulus behavior. During the cooling stage, the elastic modulus markedly rose from 1400 °C down to 1000 °C (Fig. 1a). Further sintering and the liquid viscosity increase (until it completely solidified) resulted in the material's stiffening. Finally, below 1000 °C, the *E* value showed a slow and gradual increase as the temperature was reduced.

When the second thermal cycle was performed for the cement free castables, a small decrease of E was observed up to 1000 °C, whereas above this temperature the elastic modulus dropped faster (Fig. 3). The XRD results after the second thermal cycle showed only spinel and alumina in the evaluated samples, indicating that silica fume might be present as a glassy phase with other oxides. During the cooling step, the decrease in the temperature and the liquid phase solidification resulted in an increase in the elastic modulus. Additionally, no changes in the curve′s profile was detected, indicating that the main transformations for thermal treatments in the 50–1400 °C temperature range have already been completed (Fig. 3).

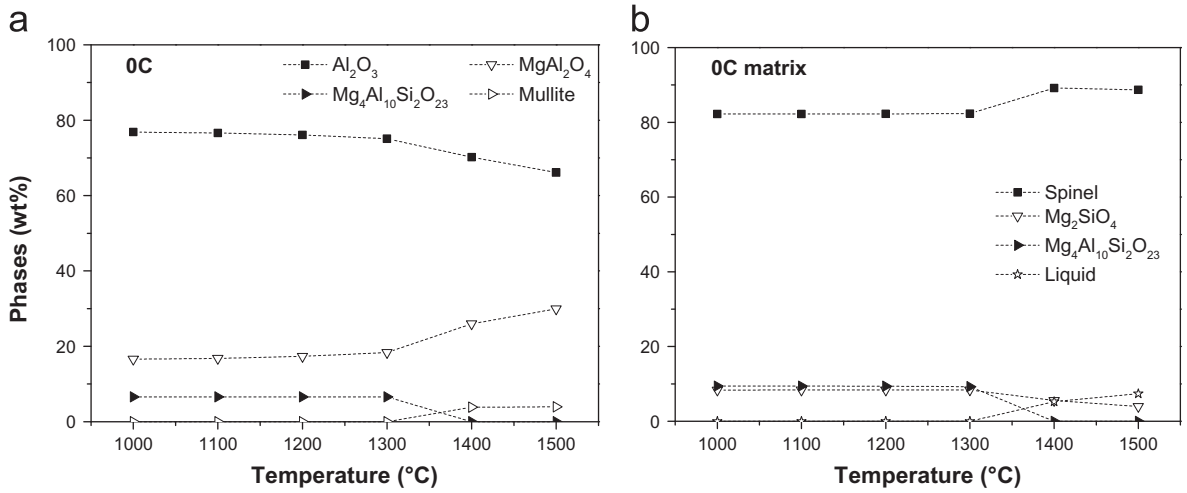


Fig. 2. Thermodynamic predictions of the phases contained in the 0C refractory castable (a) and its fine matrix (b) as a function of the temperature.

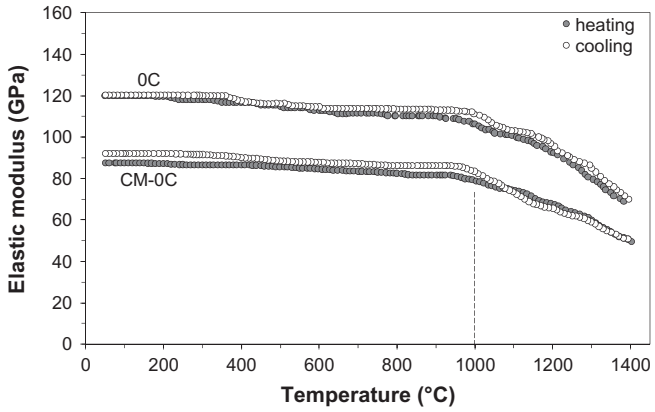


Fig. 3. *In situ* elastic modulus evolution (2nd thermal cycle) for the castables without cement and containing dead-burnt or caustic magnesia (0C and CM-0C).

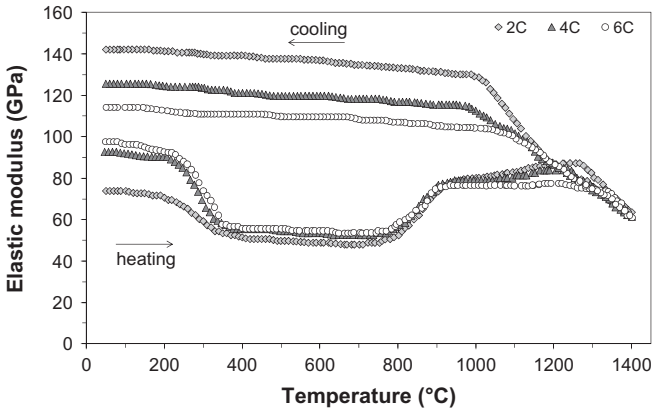


Fig. 4. *In situ* elastic modulus as a function of the temperature for the castables containing calcium aluminate cement and dead-burnt magnesia (2C, 4C and 6C). Samples obtained after curing (50 °C/24 h) and drying (110 °C/24 h) steps.

Therefore, based on the previous results for the cement free castables, it was concluded that caustic magnesia did not speed up the expected reactions whereas the dead burnt magnesia resulted in higher *E* values for all the temperature range evaluated. Furthermore, this DB MgO source presents lower amounts of impurities, which significantly affect the liquid formation starting temperature and its total content. Considering that the dead burnt magnesia containing samples attained more promising results, this MgO source was selected for the further evaluation of the alumina–magnesia castables containing calcium aluminate cement.

### 3.2. Cement-containing $Al_2O_3$–MgO castables

Fig. 4 presents the elastic modulus (*E*) results as a function of temperature for the alumina–magnesia (DB) castables containing 2 wt%, 4 wt% or 6 wt% of calcium aluminate cement (CAC). As shown in Table 5, after drying at 110 °C the 6C castable matrix contained $Al_2O_3$, MgO, $C_3AH_6$ and $AH_3$ (where C = CaO; A = $Al_2O_3$ and H = $H_2O$) in its composition, therefore, the initial E drop during the heating stage (up to 400 °C) was mainly associated to the withdrawal of chemically bonded water of the cement hydrated phases (Fig. 4). Due to the greater content of cement hydrates, the 6C composition resulted in the highest initial elastic modulus and the greater decrease in the *E* values over this temperature range.

Although calcium aluminates dissolution lead to a significant increase in the castable pH, favoring the brucite generation [20], the presence of silica fume induces the formation of an insoluble magnesium silicate coating at the magnesia's particle surface, reducing the hydration rate and the amount of $Mg(OH)_2$ generated [21]. As a result, brucite was not detected in the CAC containing samples. In addition, the hydration of calcium aluminate cement in the presence of silica fume can also result in phases such as CASH and $Ca_3Al_2(SiO_4)_{3-x}(OH)_{4x}$ which is usually an amorphous gel and not detectable in the XRD experiments [22,23]. As previously mentioned, the initial drop in the elastic modulus was associated with the decomposition of these hydrated phases (Fig. 4).

From 400 °C up to 800 °C only a very small decrease in the *E* values was noticed (Fig. 4). This result highlighted that cement addition reduces the damage during the dewatering process, as the cement free composition showed a continuous drop in the *E* values up to 800 °C (Fig. 1a). Above this temperature,

Table 5
Phase changes in the matrix of the 6C castable obtained by X-ray diffraction analysis[a].

| Crystalline phases[b] | composition 6C | | | | |
|---|---|---|---|---|---|
| | 110 °C | 800 °C | 1000 °C | 1200 °C | 1500 °C |
| MgO | ****** | ****** | ***** | **** | ** |
| $Al_2O_3$ | ****** | ***** | **** | *** | |
| $MgAl_2O_4$ | | | ** | *** | ****** |
| $C_3AH_6$ | ** | | | | |
| $AH_3$ | ** | | | | |
| $C_{12}A_7$ | | ** | | | ** |
| CA | | * | ** | ** | |
| $CA_2$ | | | * | * | |
| $C_2AS$ | | * | * | * | * |

[a]The number of asterisks indicates the phase proportion estimated by means of the main difraction peak intensity.
[b]M = MgO; A = $Al_2O_3$; C = CaO; S = $SiO_2$ and H = $H_2O$.

remarkable changes in the attained curves for the cement bonded samples were detected (Fig. 4). $CaAl_2O_4$ (CA) crystallization usually takes place above 900 °C, but this transformation might result in a small decrease in the elastic modulus [12].

The 6C matrix presented $C_{12}A_7$, CA and a small amount of gehlenite ($Ca_2Al_2SiO_7$) at 800 °C (Table 5). As gehlenite is usually generated at higher temperatures, the results suggested that for particular situations, it might be formed by the reaction between CA and $SiO_2$, as depicted in the literature [24]. Therefore, the considerable increase in the *E* values might be associated with reactions between $SiO_2$, $Al_2O_3$ and CaO, favoring the sintering at lower temperatures (Fig. 4).

Above 1000 °C, the sintering is followed by $CA_2$ and $MgAl_2O_4$ crystallization leading to the formation of stronger bonds (Fig. 4; Table 5). The volumetric expansion related to *in situ* reactions can also generate microcracks. However, according to previous investigations [10], the addition of 1 wt% of fumed silica in cement bonded $Al_2O_3$–MgO castables inhibits the $CA_2$ expansion and favors the spinel accommodation.

Despite the castable′s stiffening at temperatures lower than usual, the formation of liquid phases resulted in a marked E drop above 1200 °C (Fig. 4). For the 2C composition, the decrease of the elastic modulus was delayed, highlighting the role of CaO on liquid formation. Therefore, phases of low-melting temperatures might have been generated due to the reactions among CaO, $SiO_2$ and $Al_2O_3$. Increasing the temperature, the liquid phase viscosity is usually reduced and, as a consequence, the elastic modulus decreases. It should be emphasized that the samples were kept at the maximum temperature (1400 °C) for only 10 min, therefore, the amount of $CA_6$ generated was very small and did not affect the results (Fig. 4).

CA, $CA_2$ and $C_2AS$ were detected in the 6C matrix at 1000 °C and 1200 °C, whereas $CA_6$ was not observed at 1500 °C. Moreover, the limited amount of alumina in the evaluated matrix (comprising raw materials that presented particle sizes lower than 100 μm; Table 3), favored $C_{12}A_7$ crystallization during the liquid phase solidification (Table 5).

In order to better understand the elastic modulus results, the phases predicted to be found under equilibrium condition in the overall composition and the fine castable matrices were also simulated. Although some differences between the thermodynamic calculations and the XRD results are expected, as the reactions velocity can be low and the equilibrium condition cannot be attained, these results usually provide insights about the liquid phase generated, its composition and the transformations occurring under equilibrium state.

A considerable amount of $CA_6$ was predicted as the cement content was increased in the castable composition (Fig. 5a–c). Small amounts of melilite and anorthite were also detected. However, these phases were not identified in the XRD evaluations, showing that the equilibrium condition was not attained. By increasing the temperature (1500 °C), melilite and anorthite were consumed and the liquid formation was estimated (Fig. 5a–c).

For the castable matrices, the presence of different silica containing phases was observed in the thermodynamic calculation results (Fig. 5d–f), whereas above 1300 °C, those compounds and a small content of spinel were consumed, giving rise to the liquid formation. MgO solid solution (containing very small quantities of $Al_2O_3$ and CaO) was also detected for all evaluated matrices. Nevertheless, compared with the XRD results (Table 5), the simulations did not predict gehlenite and $C_{12}A_7$ (Fig. 5d–f), which again confirms that the samples did not attain the equilibrium condition.

The thermodynamic calculations also predicted that a higher amount of liquid phase should be found in the overall castables and their matrices at 1500 °C. The greater the cement content, the higher the liquid amount in the matrix samples would be (Table 6). As a consequence, the liquid phase became poorer in MgO and $SiO_2$, whereas the $Al_2O_3$ and CaO contents increased. On the other hand, the lower the $SiO_2$ content, the lower the viscosity was (Table 6), which can drastically affect the castable′s hot elastic properties. Despite the greater amount of liquid predicted for the 6C composition, its elastic modulus at 1400 °C was similar to the 4C and 2C ones.

Compared with the thermodynamic predictions (Fig. 5), the elastic modulus results indicated that the liquid formation took place at lower temperatures (Fig. 4). As previously mentioned, such differences must be a consequence of the impurities contained in the raw materials and the changes in the local domains composition throughout the microstructure. Furthermore, a recent study also indicated that the development of the phases in the $Al_2O_3$–CaO–$SiO_2$ system is much more complex than previously suggested in the literature [25]. Very small amounts of impurities such as $Na_2O$ and $Fe_2O_3$ usually presented in the alumina, cement, magnesia and fumed silica grains drastically shift the phase equilibrium and the liquid formation starting temperature [25].

During the first part of the cooling stage (from 1400 °C to 1000 °C), the *E* values for the studied castables increased considerably (Fig. 4). Such behavior was related to the increase in liquid phase viscosity until its solidification. Below 1000 °C, all samples showed the same profile and a very slow stiffening rate. On the other hand, the 2C composition presented a final elastic modulus value higher than the 4C and 6C ones, which was associated with the lower amount of

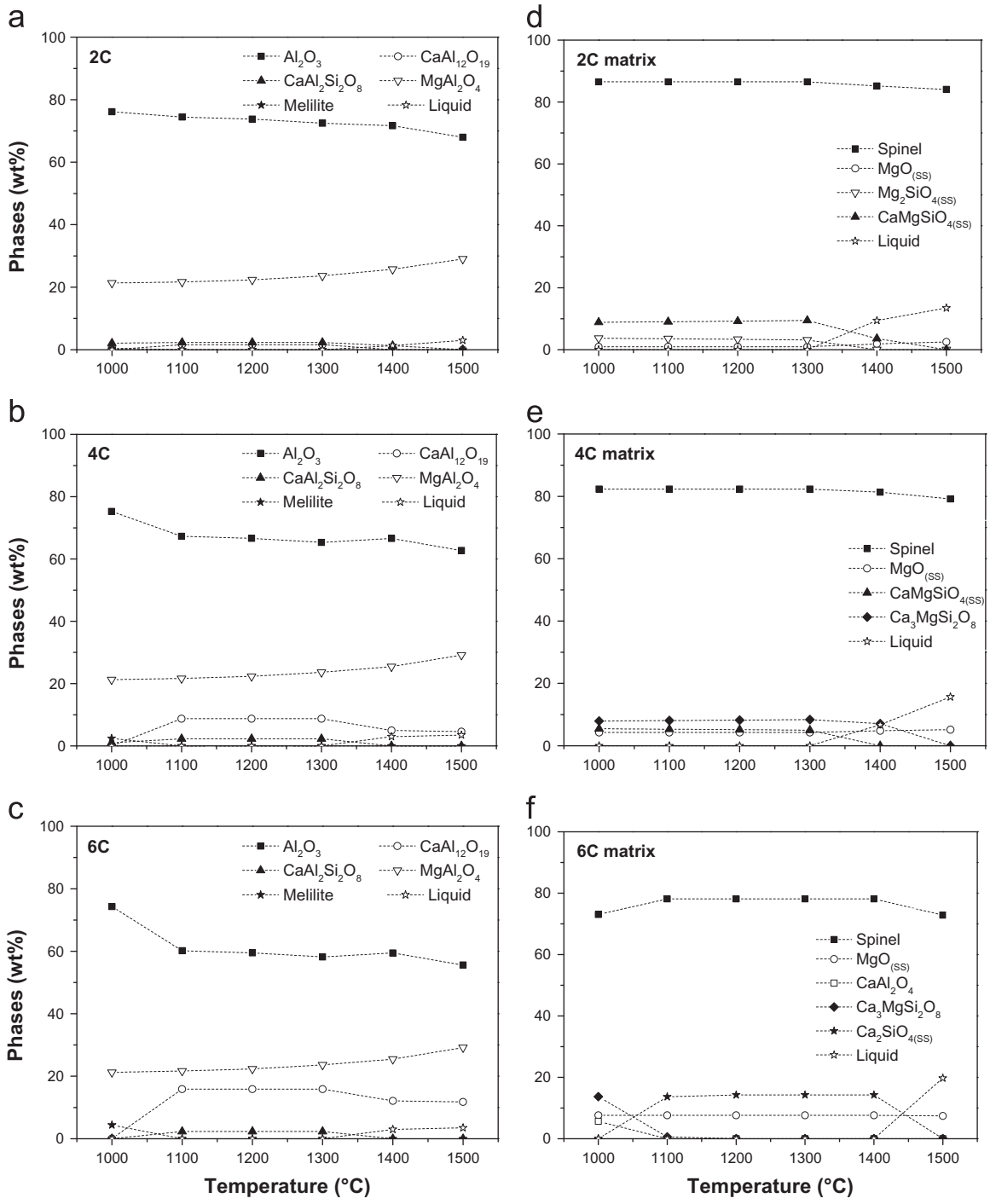


Fig. 5. Thermodynamic predictions of the phases contained in the refractory castables (a)–(c) and their fine grain matrices (d)–(f) as a function of temperature.

glassy phases that usually present lower elastic modulus than the crystalline ones. Additionally, as the *E* values did not drop during the cooling step, the castables did not present a significant expansion mismatch between the phases [26].

As noticed in Fig. 6, the elastic modulus results collected throughout the second thermal cycle showed very similar profiles for all evaluated castables. During the heating stage, a slight drop of the *E* values was observed up to 1000 °C and, above this temperature, it decreased reaching the lowest value at 1400 °C. Therefore, it could be speculated that a glassy phase transition took place around 1000 °C. Comparing the cement bonded composition′s profiles between 1400 °C to 1000 °C (Fig. 6), a small hysteresis was observed for the 4C and 2C castables. As the amount of liquid phase in the matrices at high temperature and their phase compositions significantly change with the increase in the cement content (Table 6), thus the hysteresis observed in the E profiles might be mainly associated with the glassy phase generated and its solidification.

The main phases identified in the alumina–magnesia cement bonded castables after the second thermal cycle of elastic modulus

Table 6
Thermodynamic predictions of the liquid phase composition contained in the refractory castables (6C, 4C and 2C) and their fine grain matrices (particles < 100 μm) at 1500 °C.

| Liquid at 1500 °C | | Amount (wt%) | Viscosity (Pa s) | Liquid composition (%) | | | |
|---|---|---|---|---|---|---|---|
| | | | | $Al_2O_3$ | CaO | MgO | $SiO_2$ |
| Refractory castable | 2C | 3.0 | 1.18 | 40.7 | 20.0 | 6.0 | 33.3 |
| | 4C | 3.48 | 0.82 | 43.7 | 23.3 | 4.3 | 28.7 |
| | 6C | 3.48 | 0.82 | 43.7 | 23.3 | 4.3 | 28.7 |
| Matrix | 2C | 13.46 | 0.23 | 13.2 | 22.3 | 27.4 | 37.1 |
| | 4C | 15.67 | 0.19 | 14.4 | 38.3 | 15.4 | 31.9 |
| | 6C | 19.74 | 0.17 | 19.2 | 45.6 | 9.9 | 25.3 |

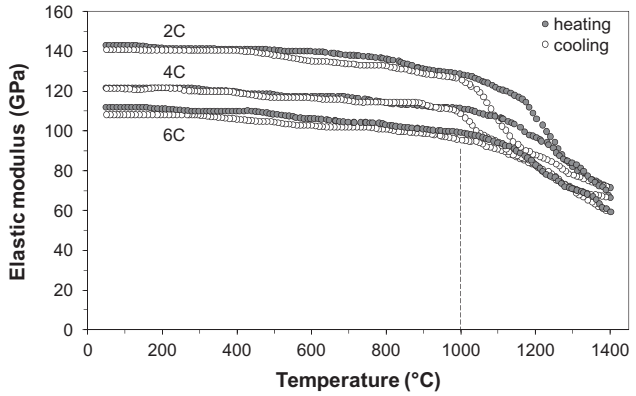


Fig. 6. *In situ* elastic modulus evolution (2nd thermal cycle) for the castables containing dead-burnt magnesia and calcium aluminate cement (2C, 4C and 6C).

measurements were spinel and alumina, but small amounts of $CA_2$, $CA_6$ and $C_2AS$ were also detected in the 4C and 6C castables. The presence of $C_2AS$ supported the previous discussions concerning the formation of low-melting temperature phases.

## 4. Conclusions

This work confirmed that the hot elastic modulus is a very suitable technique to assess *in situ* transformations in the $Al_2O_3$–MgO–CaO–$SiO_2$ and $Al_2O_3$–MgO–$SiO_2$ systems. The elastic behavior of dried and pre-fired samples was successfully investigated, highlighting the main microstructural changes (hydrated phases decomposition, spinel and $CA_2$ formation) in these refractory castables.

The MgO effect on the elastic modulus of cement free castables was evaluated by comparing compositions containing different magnesia sources (a dead burnt and a caustic one) and the following conclusions can be drawn: (i) the greater the Mg $(OH)_2$ generated, the larger the drop in the sample′s stiffness during its decomposition; (ii) the spinel formation can induce a significant rise in the elastic modulus values above 1000 °C; and (iii) the reactivity of fine magnesia sources did not significantly affect the castable behavior at high temperature.

For the alumina–magnesia cement bonded system, the attained results indicated that reactions between $SiO_2$, $Al_2O_3$ and CaO play an important role on the castable′s elastic modulus behavior, resulting in a remarkable increase in the *E* values at temperatures lower than the usual one (800 °C). On the other hand, such reactions also lead to liquid phase generation at higher temperatures (1200 °C), spoiling the hot elastic properties.

Thermodynamic calculations and XRD analysis were useful to confirm the transformations detected in the *in situ* E measurements. In addition, these results provided evidence for the liquid phase generated in the evaluated compositions. Thus, the change in the elastic modulus observed at high temperatures should be a consequence of liquid formation, suggesting that a glassy phase transition occurred above 1000 °C for all the studied castables. According to the thermodynamic calculation, reducing the cement content a lower amount of glassy phase was generated in the matrix, leading to a higher *E* value after the cooling stage. The increase of the glassy phase content weakened the materials, as it usually presents lower elastic modulus than the crystalline ones.

## Acknowledgments

The authors are grateful to the Magnesita Refratários S.A. (Brazil), FIRE, FIPAI and CNPq for supporting this work.

## References

[1] J.B. Wachtman Jr., D.G. Lam Jr., Young′s modulus of various refractory materials as a function of temperature, Journal of the American Ceramic Society 42 (5) (1959) 254–260.
[2] J. Gajda, D. Mcgee, Elastic properties of calcium aluminate-cement-based concrete, American Ceramic Society Bulletin 76 (4) (1997) 81–85.
[3] E. Nonnet, N. Lequeux, P. Boch, Elastic properties of high alumina cement castables from room temperature to 1600 °C, Journal of the European Ceramic Society 19 (1999) 1573-1583.
[4] G.K. Layden, G.W. Brindley, Kinetics of vapor-phase hydration of magnesium oxide, Journal of the American Ceramic Society 46 (11) (1963) 518–522.
[5] R. Salomão, L.R. Bittencourt, V.C. Pandolfelli, A novel approach for magnesia hydration assessment in refractory castables, Ceramics International 33 (2007) 803–810.
[6] M.A. Braulio, D.H. Milanez, E.Y. Sako, L.R.M. Bittencourt, V.C. Pandolfelli, Expansion behavior of cement-bonded alumina–magnesia refractory castables, American Ceramic Society Bulletin 86 (12) (2007) 9201–9206.
[7] T.M. Souza, M.A.L. Braulio, A.P. Luz, P. Bonadia, V.C. Pandolfelli, Systemic analysis of MgO hydration effects on alumina–magnesia refractory castables, Ceramics International 38 (2012) 3969–3976.
[8] M.A. Braulio, L.R.M. Bittencourt, V.C. Pandolfelli, Magnesia grain size effect on in situ spinel refractory castables, Journal of the European Ceramic Society 28 (2008) 2845–2852.
[9] M.A. Braulio, J.F.R. Castro, C. Pagliosa, L.R.M. Bittencourt, V.C. Pandolfelli, From macro to nano magnesia: designing the in situ spinel expansion, Journal of the American Ceramic Society 91 (9) (2008) 3090–3093.
[10] M.A. Braulio, L.R.M. Bittencourt, J. Poirier, V.C. Pandolfelli, Microssilica effects on cement bonded alumina–magnesia refractory castables, Journal of Technologies Associates Refraction Jnp 28 (3) (2008) 180–184.

[11] M.A.L. Braulio, V.C. Pandolfelli, Tailoring the microstructure of cement-bonded alumina–magnesia refractory castables, Journal of the American Ceramic Society 93 (2010) 2981–2985.
[12] J.M. Auvray, C. Gault, M. Huger, Evolution of elastic properties and microstructural changes versus temperature in bonding phases of alumina and alumina–magnesia refractory castables, Journal of the European Ceramic Society 27 (2007) 3489–3496.
[13] J.M. Auvray, C. Gault, M. Huger, Microestructural changes and evolutions of elastic properties versus temperature of alumina and alumina–magnesia refractory castables, Journal of the European Ceramic Society 28 (2008) 1953–1960.
[14] M.A.L. Braulio, D.H. Milanez, E.Y. Sako, L.R.M. Bittencourt, V.C. Pandolfelli, The effect of calcium aluminate cement content on the in-situ spinel expansion, in: Proccedings of UNITECR'07, Dresden, Alemanha, 2007, pp. 540–543.
[15] R.G. Pileggi, A.R. Studart, M.D.M. Innocentini, V.C. Pandolfelli, High performance refractory castables, American Ceramic Society Bulletin 81 (2002) 37–42.
[16] G. Pickett, Equations for computing elastic constants from flexural and torsional resonant frequencies of vibration of prisms and cylinders, Proceedings of the American Society for Testing and Materials 45 (1945) 846–865.
[17] R. Salomão, V.C. Pandolfelli, Magnesia sinter hydration–dehydration behavior in refractory castables, Cerâmica 54 (2008) 145–151 (in Portuguese).
[18] A. Hundere, B. Myhre, C. Odegard, B. Sandberg, Magnesium-silicate-hydrate bonded $MgO–Al_2O_3$ castables, in: Annual Conference of Metallurgists, Symposium Advances in Refractories for the Metallurgical Industries III, Quebec, Canada, 1999.
[19] B. Sandberg, B. Myhre, J.L. Holm, Catables in the system $MgO–Al_2O_3–SiO_2$, in: Unified International Technical Conference Refractories UNITECR'95 Kyoto Japan, 1995.
[20] R. Salomão, V.C. Pandolfelli, The role of hydraulic binders on magnesia containing refractory castables: calcium aluminate cement and hydratable alumina, Ceramics International 35 (2009) 3117–3124.
[21] R. Salomão, V.C. Pandolfelli, Microsilica addition as anti-hydration tecnique of magnesia in refractory castables, Cerâmica 54 (2008) 43–48 (in Portuguese).
[22] J.M.R. Mercury, X. Turrillas, A.H. de Aza, P. Pena, Calcium aluminates hydration in presence of amorphous $SiO_2$ at temperatures below 90 °C, Journal of Solid State Chemistry 179 (2006) 2988–2997.
[23] P.S. Silva, F.P. Glasser, Phase relations in the system $CaO–Al_2O_3–SiO_2–H_2O$ relevant to metakaolin—calcium hydroxide hydration, Cement and Concrete Research 23 (1993) 627–639.
[24] S. Goberis, I. Pundene, A. Shpokauaskas, T. Wala, Microsilica tested as a component for the binder of a medium-cement refractory castable, Refractories and Industrial Ceramics 44 (4) (2003) 205–210.
[25] E.Y. Sako, M.A.L. Braulio, E. Zinngrebe, S.R. van der Laan, V.C. Pandolfelli, In depth microstructural evolution analyses of cement-bonded spinel refractory castables: novel insights regarding spinel and $CA_6$ formation, Journal of the American Ceramic Society 95 (5) (2012) 1732–1740.
[26] A.P. Luz, T. Santos Jr., J. Medeiros, V.C. Pandolfelli, Thermal shock damage evaluation of refractory castables via hot elastic modulus measurements, Ceramics International 39 (2013) 6189–6197.